Squark cascade decays to charginos/neutralinos: Gluon radiation

R. Horsky and M. Krämer
Institut für Theoretische Physik E, RWTH Aachen U., D-52056 Aachen, Germany

A. Mück
Paul Scherrer Institut, Würenlingen und Villigen, Ch-5232 Villigen PSI, Switzerland

P. M. Zerwas
Institut für Theoretische Physik E, RWTH Aachen U., D-52056 Aachen, Germany
Deutsches Elektronen–Synchrotron DESY, D–22603 Hamburg, Germany
Laboratoire de Physique Théorique, U. Paris-Sud, F-91405 Orsay, France
(Received 1 April 2008; published 8 August 2008)

The momentum spectrum and the polarization of charginos and neutralinos in squark decays are affected by gluon radiation in the decay process $\tilde{q} \to q\tilde{\chi}(g)$. We determine these corrections and study their impact on the $[q\ell]$ invariant mass distributions for leptonic $\tilde{\chi}$ decays. The higher-order corrections, though small in general, can be sizeable near pronounced edges of the final-state distributions.

DOI: 10.1103/PhysRevD.78.035004 PACS numbers: 12.60.Jv

I. INTRODUCTION

The properties of supersymmetric particles, colored and noncolored, can be studied at the Large Hadron Collider (LHC) in cascade decays of squarks and gluinos, which have large production cross sections in high-energy hadron collisions. In particular, squarks that are lighter than gluinos decay exclusively to quarks and charginos or neutralinos, $\tilde{q} \to q\tilde{\chi}$. Subsequent decays of neutralinos into final states with two leptons are especially well suited to investigate properties of the supersymmetric spectrum. Invariant mass distributions of the final-state leptons and jets can be exploited, for example, for precision measurements of supersymmetric particle masses (see e.g. [1–4]). Moreover, correlations among the particles in the decay chains allow spin measurements of intermediate particles [5–8].

In the present article we concentrate on one aspect in the multitude of theoretical challenges involved in the description of supersymmetric cascade decays, i.e. the super-QCD (SQCD) radiative corrections at next-to-leading order (NLO) and their impact on energy distributions, polarization degrees, and on the shape of quark-lepton invariant mass distributions. Precise theoretical predictions for the shape of the distributions are required also at some distance away from kinematic edges and thresholds as to allow for sufficiently large, statistically significant event samples. Moreover, the shapes may be needed to resolve possible ambiguities in mass determinations from kinematic end points [9], they are crucial for the spin determination [5], and they allow one to test models of supersymmetry breaking [10]. We investigate the impact of QCD radiation on the shape of distributions in NLO perturbation theory and derive, largely, analytical results which provide us with the proper understanding of the SQCD effects. Extending the Monte Carlo calculation of QCD effects in Ref. [11], we include gluon radiation off the final-state quarks. (Hadronic jet fragmentation which must finally be added is beyond the scope of the present study, but the effect can be estimated by means of QCD power corrections.)

We shall, for definiteness, focus on cascades of L-type squarks, $\tilde{q}_L$, of the first two generations without noticeable L/R mixing and consider the decay chain

$$\tilde{q}_L \to q\tilde{\chi}_2^0 \to q\ell\tilde{\ell}_R \to q\ell\ell\tilde{\chi}_1^0, \tag{1.1}$$

which has been discussed in great detail in the literature for the SPS1a/a′ benchmark points [12,13]. The neutralino $\tilde{\chi}_1^0$ is assumed to be the lightest supersymmetric particle (LSP) and thus is stable in R-parity conserving theories. Since the Born terms can be factored out, the NLO analysis applies, without modifications, to all neutralino and chargino decay chains of the same form. R-type squarks, $\tilde{q}_R$, decay in large parts of the supersymmetric parameter space, particularly at the benchmark points SPS1a/a′, to the LSP, $\tilde{q}_R \to q\tilde{\chi}_1^0$, and do not develop cascades.

Spin correlations are important for the proper description of the cascade decay (1.1). Since only the gaugino components of the neutralino $\tilde{\chi}_2^0$ couple effectively to the squark/quark current if quark masses are neglected, the $\tilde{q}_L$ squarks decay to left-handedly polarized q_L quarks. By angular momentum conservation also the neutralino $\tilde{\chi}_2^0$ is polarized left-handedly at the Born level. Gluon radiation in the decay process leads to the admixture of right-handed neutralinos. The polarization is reflected in the energy and angular distributions of the decay products.

The paper is organized as follows. In Sec. II we shall present the results for the NLO SQCD corrections to the decay $\tilde{q}_L \to q\tilde{\chi}$ and their impact on the $\tilde{\chi}$ energy distribution and polarization. The phenomenology of the complete $\tilde{q}_L$ decay chain (1.1), including the spin correlations, is

discussed in Sec. III A. In Sec. III B we analyze the decay chains in the broader framework of squark production at the LHC, including R-squarks and antisquarks. We conclude in Sec. IV.

II. SUPERSYMMETRIC QCD CORRECTIONS TO THE DECAY $\tilde{q} \to q\tilde{\chi}$

Squark and gluino decays are affected by SQCD corrections. For their mutual decay modes, dominating if kinematically allowed, the NLO corrections were determined in Ref. [14]. The SQCD corrections to the partial widths for the electroweak squark decay channels,

$$\tilde{q} \to q + \tilde{\chi} + (g), \tag{2.1}$$

were calculated in Refs. [15–18]: Virtual gluon and gluino/squark exchanges renormalize the $q\tilde{q}\,\tilde{\chi}$ vertex and additional gluons are radiated in the final state, *cf.* Fig. 1.

Vertex corrections neither change the $\tilde{\chi}$ momentum nor its polarization state, but both are affected by gluon radiation. The $\tilde{\chi}$ line spectrum of the two-body decay becomes a continuous spectrum (Sec. II A). Since in radiative decays the $\tilde{\chi}$ is not back-to-back anymore with the polarized zero-mass quark q, spin-flipped $\tilde{\chi}$ states are admixed (Sec. II B). While the effect on the polarization is small, the overall impact of gluon radiation on the final-state distributions, particularly near edges, is quite significant, *nota bene* in view of the envisaged high-precision analyses of these cascade modes at the LHC.

A. $\tilde{\chi}$ energy distribution

Gluon radiation reduces the scaled energy $x_{\tilde{\chi}} = 2E_{\tilde{\chi}}/M_{\tilde{q}}$ of the neutralino in the unpolarized decay $\tilde{q} \to q\tilde{\chi}(g)$ in the squark rest frame according to the distribution

$$\frac{1}{\Gamma_B}\frac{d\Gamma}{dx_{\tilde{\chi}}} = \frac{4}{3}\frac{\alpha_s}{\pi}\frac{1}{(1-\kappa)^2}\frac{1}{1+\kappa-x_{\tilde{\chi}}}\Big[(1-\kappa)(2-x_{\tilde{\chi}}) \times \log\Big(\frac{2-x_{\tilde{\chi}}+p_{\tilde{\chi}}}{2-x_{\tilde{\chi}}-p_{\tilde{\chi}}}\Big) + \frac{1}{4}p_{\tilde{\chi}}(x_{\tilde{\chi}}-8+6\kappa)\Big]. \tag{2.2}$$

The energy fraction $x_{\tilde{\chi}}$ varies between the minimum $2\sqrt{\kappa}$ and the maximum value $1+\kappa$. A useful abbreviation has been introduced for the mass ratio, $\kappa = M_{\tilde{\chi}}^2/M_{\tilde{q}}^2$, with $M_{\tilde{\chi}/\tilde{q}}$ being the $\tilde{\chi}/\tilde{q}$ masses; $p_{\tilde{\chi}} = \sqrt{x_{\tilde{\chi}}^2 - 4\kappa}$ denotes the scaled neutralino momentum in the squark rest frame. The distribution is normalized to the partial width in Born approximation, Refs. [16,17],

$$\Gamma_B = \frac{\alpha}{4}M_{\tilde{q}}(1-\kappa)^2 f_{\tilde{q}\tilde{\chi}}^2, \tag{2.3}$$

depending on the chargino and neutralino mixing parameters [19,20] in the coefficients $f_{\tilde{q}\tilde{\chi}}$.

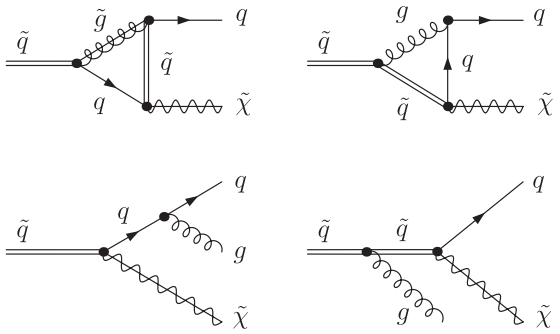

FIG. 1. Generic Feynman diagrams for virtual and real super-QCD corrections to the decay $\tilde{q} \to q\tilde{\chi}$.

Collinear and infrared gluon emission, the leading part accounted for by the logarithmic term in Eq. (2.2), generate singularities at the maximum $\tilde{\chi}$ energy $x_{\tilde{\chi}} \to x_{\tilde{\chi}}^{\max} = 1+\kappa$. The leading contribution in $\delta = x_{\tilde{\chi}}^{\max} - x_{\tilde{\chi}}$ can be resummed by applying techniques analogous to thrust distributions [21–24]:

$$\frac{1}{\Gamma_B}\frac{d\Gamma}{dx_{\tilde{\chi}}} \simeq \frac{4}{3}\frac{\alpha_s}{\pi}\frac{1}{\delta}\Big[\log\frac{1}{\delta}+c\Big] \Rightarrow \frac{4}{3}\frac{\alpha_s}{\pi}\frac{1}{\delta}\Big[\log\frac{1}{\delta}+c\Big] \times \exp\Big[-\frac{4}{3}\frac{\alpha_s}{\pi}\Big(\frac{1}{2}\log^2\frac{1}{\delta}+c\log\frac{1}{\delta}\Big)\Big] \tag{2.4}$$

with the subleading coefficient

$$c = -\frac{7}{4} + \frac{\log[(1-\kappa)^2]}{(1-\kappa)^2}. \tag{2.5}$$

Multiple gluon emission bends the distribution to zero at the kinematical boundary, corresponding to the Sudakov suppression of a final state without any gluons. Depending in detail on the effective value of α_s, the turnover point is very close to the maximum of $x_{\tilde{\chi}}$.

The $\tilde{\chi}$ energy distribution is displayed in Fig. 2(a) for L-squark decays to $\tilde{\chi}_2^0$, with parameters adopted from SPS1a′ (i.e. $\kappa = 0.108$) and the QCD coupling set to $\alpha_s(M_{\tilde{q}}) = 0.093$.

The value of the average $\tilde{\chi}$ energy for the inclusive NLO prediction is obtained by integration over the energy spectrum including the 2-body decay limit. Both, the QCD corrected 2-body and the 3-body part of the calculation are infrared divergent, the singularities canceling each other mutually. Analogously to the methods employed in Refs. [16,17], small quark and gluon masses are introduced to regularize the singularities. The averaged observable $\langle x_{\tilde{\chi}}\rangle$ reflects the deviation from the Born prediction to order α_s:

$$\langle x_{\tilde{\chi}}\rangle = x_{\tilde{\chi}}^{\max} - \frac{1}{9}\frac{\alpha_s}{\pi}\frac{1}{(1-\kappa)^2}[(1-\kappa)(4-\kappa[17-7\kappa]) - 6(2-\kappa)\kappa^2\log\kappa]. \tag{2.6}$$

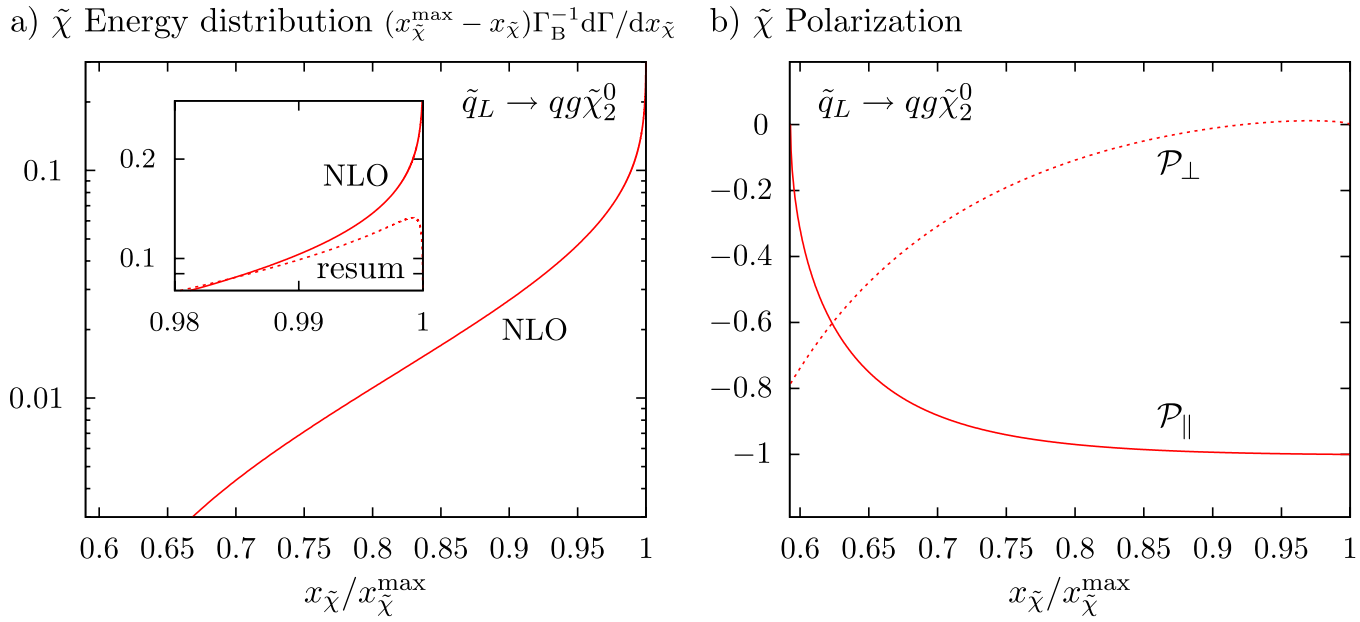

FIG. 2 (color online). (a) The differential decay rate for $\tilde{q}_L \to q g \tilde{\chi}_2^0$ as a function of the $\tilde{\chi}_2^0$ energy $x_{\tilde{\chi}}$ at the benchmark point SPS1a′ ($M_{\tilde{\chi}}/M_{\tilde{q}} = 0.329$). The curve labeled "resum" shows the damping near $x_{\tilde{\chi}}^{\max}$ from multiple gluon radiation according to Eq. (2.4). (b) The longitudinal and transverse polarization of the neutralino $\tilde{\chi}_2^0$.

For the reference point SPS1a′ ($\kappa = 0.108$) adopted in the numerical analyses of the next section, the mass-dependent coefficient of the $\mathcal{O}(\alpha_s)$ contributions takes the value

$$\langle x_{\tilde{\chi}} \rangle = x_{\tilde{\chi}}^{\max} - 0.32 \frac{\alpha_s}{\pi}. \tag{2.7}$$

Thus, the average $\tilde{\chi}$ energy is reduced due to gluon radiation at the percent level.

B. $\tilde{\chi}$ polarization vector

Gluon radiation at NLO also affects the $\tilde{\chi}$ polarization. At the Born level the $\tilde{\chi}$ polarization in $\tilde{q}_L$ decays must be left-handed. While the $\tilde{\chi}$ spin does not flip for collinear and infrared gluon emission, because the intermediate left-chiral quark is effectively on-shell in these configurations, the $\tilde{\chi}$ spin can flip for noncollinear/noninfrared final-state configurations, with the angular momentum balanced by the emitted hard gluon.

The polarization vector $\vec{\mathcal{P}}[\tilde{\chi}]$ is defined in the $\tilde{\chi}$ rest frame. The x axis is chosen as the $\tilde{\chi}$ flight direction in the $\tilde{q}$ rest frame, the $[x, y]$ plane is identified, for 3-particle final states, with the $\tilde{\chi}\,\tilde{q}$ decay plane, the y axis pointing to the half-plane of shortest rotation from the $\tilde{\chi}$ to the q momentum vector. The polarization vector lies within the decay plane, with components parallel, $\mathcal{P}_\parallel = \mathcal{P}_x$, and transverse, $\mathcal{P}_\perp = \mathcal{P}_y$, to the $\tilde{\chi}$ flight direction while the perpendicular polarization component vanishes ($\mathcal{P}_z = 0$).

The two components of the polarization vector for fixed $x_{\tilde{\chi}}$ can be cast into the form

$$\begin{aligned}
\mathcal{P}_\parallel(x_{\tilde{\chi}}) &= \frac{1}{4}\frac{1}{(1-\kappa)^2}\frac{1}{(1+\kappa-x_{\tilde{\chi}})p_{\tilde{\chi}}}\Big[4(2-x_{\tilde{\chi}}) \\
&\quad \times (\kappa[4-x_{\tilde{\chi}}]-x_{\tilde{\chi}})\log\Big(\frac{2-x_{\tilde{\chi}}+p_{\tilde{\chi}}}{2-x_{\tilde{\chi}}-p_{\tilde{\chi}}}\Big) \\
&\quad + ([8-x_{\tilde{\chi}}]x_{\tilde{\chi}} - 4\kappa[7-2x_{\tilde{\chi}}])p_{\tilde{\chi}}]/\mathcal{N}, \\
\mathcal{P}_\perp(x_{\tilde{\chi}}) &= \frac{\pi}{8}\frac{1}{(1-\kappa)^2}\frac{\sqrt{\kappa}}{\sqrt{1+\kappa-x_{\tilde{\chi}}}p_{\tilde{\chi}}}[32+20\kappa \\
&\quad - 16\sqrt{1+\kappa-x_{\tilde{\chi}}}(2-x_{\tilde{\chi}}) \\
&\quad - x_{\tilde{\chi}}(32-3x_{\tilde{\chi}})]/\mathcal{N}.
\end{aligned} \tag{2.8}$$

The normalization factor $\mathcal{N}$ denotes the distribution $(\frac{4}{3} \times \frac{\alpha_s}{\pi}\Gamma_B)^{-1} d\Gamma/dx_{\tilde{\chi}}$ at the point $x_{\tilde{\chi}}$. For fixed $x_{\tilde{\chi}} < x_{\tilde{\chi}}^{\max}$ the polarization vector is independent of α_s to leading order and depends only on the radiation dynamics.

In the infrared and collinear limits of gluon radiation, $x_{\tilde{\chi}} \to x_{\tilde{\chi}}^{\max}$, the Born values are approached again,

$$\begin{aligned}
\mathcal{P}_\parallel &\to -1 + \frac{\kappa}{2(1-\kappa)^2}\frac{\delta}{\log(1/\delta)} \to -1, \\
\mathcal{P}_\perp &\to \frac{3\pi}{8}\frac{\sqrt{\kappa}}{(1-\kappa)}\frac{\sqrt{\delta}}{\log(1/\delta)} \to 0.
\end{aligned} \tag{2.9}$$

In the opposite limit, $x_{\tilde{\chi}} \to x_{\tilde{\chi}}^{\min} = 2\sqrt{\kappa}$, the polarization components approach the values $\mathcal{P}_\parallel \to 0$ and $\mathcal{P}_\perp \to -\pi/4$. The two components of the polarization vector are displayed in Fig. 2(b), again for the mass pattern of the SPS1a′ scenario ($\kappa = 0.108$).

The values of the average polarization components of $\tilde{\chi}$ including the inclusive NLO contributions can easily be calculated. Since the polarization effects are not infrared-sensitive, the only divergent integrals are those already encountered in the unpolarized results. The averaged observables $\langle \mathcal{P}_\parallel \rangle$, and $\langle \mathcal{P}_\perp \rangle$ are given by

$$\begin{aligned}\langle \mathcal{P}_\parallel \rangle &= -1 - \frac{1}{9}\frac{\alpha_s}{\pi}\frac{1}{(1-\kappa)^2}[4\pi^2(\kappa-3)\kappa \\ &\quad - 48(\kappa-3)\kappa \mathrm{Li}_2(\sqrt{\kappa}) + 12(1-\kappa[8-3\kappa])\mathrm{Li}_2(\kappa) \\ &\quad - 3\sqrt{\kappa}(22[1+\kappa] - \sqrt{\kappa}[45-\kappa]) \\ &\quad + 6(1-\kappa)(11-3\kappa)\log(\sqrt{\kappa}+1) \\ &\quad + 3(4[1-\kappa]^2\log(1-\kappa) + \kappa[4-3\kappa])\log\kappa], \\ \langle \mathcal{P}_\perp \rangle &= \frac{2\alpha_s}{3}\frac{\sqrt{\kappa}}{(1-\kappa)^2}[4 + 4\log\kappa - 4\kappa - (1+\sqrt{\kappa}) \\ &\quad \times (15-\kappa)\mathrm{E} - 2(\kappa - 7\sqrt{\kappa} - 8)\mathrm{K}]. \end{aligned} \tag{2.10}$$

The function Li_2 is the usual dilogarithm while K and E abbreviate the complete elliptic integrals of the first and second kind [25], respectively, evaluated for the argument $[(1-\sqrt{\kappa})/(1+\sqrt{\kappa})]^2$.

For the reference point SPS1a′ the coefficients of the $\mathcal{O}(\alpha_s)$ contributions take the values

$$\langle \mathcal{P}_\parallel \rangle = -1 + 0.02\frac{\alpha_s}{\pi} \quad \text{and} \quad \langle \mathcal{P}_\perp \rangle = +0.08\frac{\alpha_s}{3}. \tag{2.11}$$

The NLO SQCD effect on the average longitudinal component of the $\tilde{\chi}$ polarization vector, $\langle \mathcal{P}_\parallel \rangle$, is very small. This follows from the fact that in the collinear and infrared regions, in which the density of the Dalitz plot is maximal, the deviation of the polarization vector from the Born approximation approaches zero. The average perpendicular polarization $\langle \mathcal{P}_\perp \rangle$ is positive, dominated by the contributions from the region of large $\tilde{\chi}$ energies.

III. PHENOMENOLOGICAL RESULTS

A. The $\tilde{q}_L$ decay chain

For parameter points like SPS1a/1a′, the decays to lepton/slepton pairs of the first two generations,

$$\tilde{\chi}_2^0 \to \ell_R^+ + \tilde{\ell}_R^- \quad \text{and} \quad \ell_R^- + \tilde{\ell}_R^+, \tag{3.1}$$

are ideal spin analyzers (R denoting right chirality) since the decays into the L-type state $\tilde{\ell}_L^\pm$ are kinematically forbidden, and L/R slepton mixing as well as the $\tilde{\chi}_2^0$ Higgsino component are suppressed. (Small corrections due to nonzero lepton masses can easily be included.)

For the sake of clarity, we first focus on these $\ell_R^+\tilde{\ell}_R^-$ decay modes of the neutralino. Since the positron ℓ_R^+ is left-handedly polarized, it will be emitted preferentially antiparallel to the $\tilde{\chi}$ spin direction:

$$\frac{1}{\Gamma}\frac{d\Gamma}{d\cos\theta_s} = \frac{1}{2}(1 - \mathcal{P}[\tilde{\chi}]\cos\theta_s), \tag{3.2}$$

where θ_s is the angle between the $\tilde{\chi}$ spin vector and the ℓ^+ 3-momentum, and $\mathcal{P}[\tilde{\chi}]$ the $\tilde{\chi}$ degree of polarization. The angular correlation Eq. (3.2) gives rise to an increase of the invariant mass of the $[q\ell^+]$ pair in the decay chain

$$\tilde{q}_L \to q + \tilde{\chi}_2^0 + (g) \to q + \ell^+ + \tilde{\ell}_R^- + (g) \tag{3.3}$$

compared with the isotropic distribution. (In this cascade the lepton ℓ is generally termed "near lepton" as opposed to the "far lepton" emitted in the subsequent slepton decay $\tilde{\ell} \to \ell\tilde{\chi}_1^0$, which will be included later.)

We have implemented the NLO results presented above in a flexible parton-level Monte Carlo program to calculate arbitrary differential distributions. Both phase-space slicing and subtraction methods have been employed to allow for internal cross checks.

In the phase-space slicing approach, approximate real radiation matrix elements are integrated analytically in the soft/collinear regions using mass regularization. After adding the mass-regularized virtual corrections, the result is finite and the regulating quark and gluon masses can be set to zero. The hard gluon region is integrated by standard Monte Carlo techniques.

Alternatively, a subtraction method has been applied which is particularly suited to construct the NLO parton-level Monte Carlo program for the decay process. In the present, very simple case the entire 3-particle differential decay width can be used as a subtraction term. For the observables $\mathcal{O}$ which we consider, the expression in NLO can be cast in the form

$$\langle \mathcal{O} \rangle_{\mathrm{NLO}} = \int_3 d\hat{\Gamma}_3^R[\mathcal{O}_3 - \mathcal{O}_2] + \int_2\Big[d\hat{\Gamma}_2^V + \int_1 d\hat{\Gamma}_3^R\Big]\mathcal{O}_2. \tag{3.4}$$

Here, $d\hat{\Gamma}_3^R$ is the differential 3-parton decay width, $d\hat{\Gamma}_2^V$ the vertex-corrected 2-parton decay width, both normalized to the NLO width Γ. The observables $\mathcal{O}$ calculated for either $n=3$ or $n=2$ parton final states are denoted by $\mathcal{O}_n$. The first integral in Eq. (3.4) is finite by construction and can be integrated by Monte Carlo techniques. The second and the third integral can be evaluated analytically. The results derived by using the subtraction method agree with those obtained from phase-space slicing.

When gluon radiation is switched on, the $[q\ell^+]$ invariant mass distribution is softened. To quantify this effect, the q-jet must be defined properly in an infrared-safe way. We will combine the q and g partons in the collinear and infrared regimes to a single $\hat{q}$-jet if their scaled invariant mass $y = M^2[\hat{q} = qg]/M_{\tilde{q}}^2$ is less than $y_c = 0.01$. For events with noncollinear hard gluon emission we identify $\hat{q}$ with the leading parton jet, i.e. the jet with the highest energy in the squark rest frame, either q or, rarely, g.

The invariant mass distributions $M^2[\hat{q}\ell^{\pm}]$ are displayed as solid curves in Fig. 3. In the upper left panel the distribution of the positively charged "near" leptons, produced in $\tilde{\chi}_2^0$ decays, is shown. The dashed curve represents the invariant mass distribution at the Born level for comparison. The peak of the distribution at high invariant mass is more pronounced than the triangular-shaped tree-level distribution with spin correlations ignored [26]. As expected, the NLO corrections lead to the transfer of events to smaller invariant masses compared to the tree-level prediction.

The transition from the 1-jet to the 2-jet class of events gives rise to the tiny kink in the $[\hat{q}\ell^+_{\rm near}]$ distribution in Fig. 3. Varying the experimentally defined jet-resolution parameter $y_{\rm c}$ reproduces anticipated modifications of the mass distributions: the distribution is softened for smaller $y_{\rm c}$, and the peak rounded off, exemplified in Fig. 3 for $y_{\rm c} = 0.002$, as a larger fraction of events with respect to the default choice $y_{\rm c} = 0.01$ moves from the 1-jet to the 2-jet class. For larger $y_{\rm c}$ the distribution is sharpened, moving back towards the Born distribution, as more events are attributed to the 1-jet class. The NLO distribution becomes

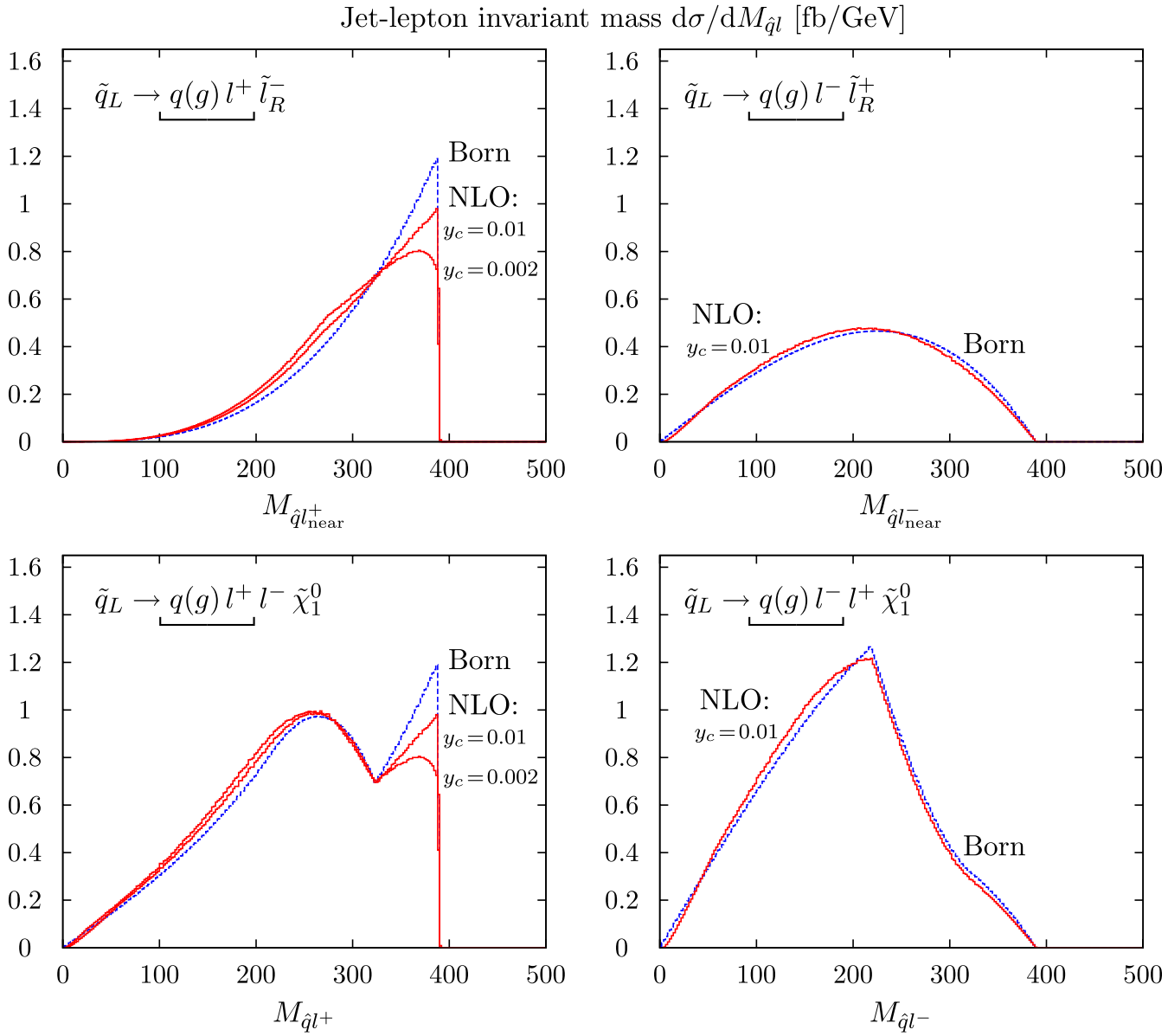

FIG. 3 (color online). The $[\hat{q}l^{\pm}]$ invariant mass distributions for positively (left panels) and negatively (right panels) charged leptons is shown at SPS1a′ (specifically for $\tilde{u}_L$ masses and first and second generation leptons with vanishing masses). The upper panels include only near leptons while the lower panels display the sum of near and far leptons. The NLO predictions are represented by the solid lines for y-cut parameters $y_{\rm c} = 0.01$ and 0.002, the Born result (approximately equivalent to NLO with $y_{\rm c} \gtrsim 0.05$) by the dashed line.

almost identical to the LO prediction for $y_c \gtrsim 0.05$. Quite similar results for the invariant mass distributions are found when using a cone algorithm [27] defined in the squark rest frame.

Parallel to the $\tilde{\chi}$ energy distribution, exponential Sudakov damping of the invariant $[\hat{q}\ell^+]$ mass distribution is expected in a margin of 1% below the pronounced kinematical edge when multiple gluon radiation is switched on. Likewise, hadronic jet fragmentation will give rise to smearing effects, generally accounted for, see e.g. Ref. [28], by shifting the perturbative prediction of the distribution downwards by a relative amount of approximately 1 GeV$/M_{\tilde{q}}$. For squarks decaying through electroweak channels, as at the present reference point, nonzero width effects $\propto \Gamma_{\tilde{q}}/M_{\tilde{q}}$ are also limited to about 1%, on both sides of the kinematical edge, though [29]. These effects will round off the peak of the distribution at the edge for $y_c \gtrsim 0.01$, with the overall impact limited however to a margin at the 1% level for squark masses in excess of 500 GeV. With details depending on the jet definition, the modification will qualitatively be similar to the thrust distribution in jet analyses of e^+e^- annihilation at high energies [28]. The explicit Monte Carlo simulation of QCD effects in Ref. [11] includes only gluon radiation off the squarks which turns out, as expected, to have a very small effect on the shape of the distributions.

The experimentally observed lepton ℓ^+ may also be the decay product of the slepton in the chain [31] $\tilde{\chi}_2^0 \to \ell_R^- \tilde{\ell}_R^+ \to \ell_R^- \ell_R^+ \tilde{\chi}_1^0$. For this "far" lepton ℓ^+, the daughter of a spinless parent, the spin characteristics in the distributions are largely washed out and only the average energy reduction of the slepton due to spin correlations in the primary neutralino decay is effective.

Adding up the contributions from near and far ℓ^+ leptons, which cannot be separated experimentally on an event-by-event basis, we arrive at the distributions displayed in the lower left panel of Fig. 3. Because of the rather small mass difference between the selectron/smuon and the LSP $\tilde{\chi}_1^0$ in SPS1a′, the lepton from the slepton decay is relatively low-energetic. Thus the far lepton adds to the distribution only at low invariant masses and the signature of the near lepton is still significant at high invariant masses.

If, instead, negatively charged leptons are observed, the shapes of the two corresponding distributions are rather different. Since the negatively charged leptons are right-handedly polarized the sign in Eq. (3.2) flips and the near ℓ^- is preferentially emitted parallel to the q-jet, in contrast to the antiparallel emission of positively charged leptons. The energy of the negatively charged lepton ℓ^- is therefore, on average, reduced in the squark rest frame for polarized $\tilde{\chi}_2^0$ decays. For both reasons, the $[\hat{q}\ell^-]$ invariant mass is reduced on average compared to the prediction without spin correlations [26]. The reduction is slightly enhanced by gluon emission as demonstrated in the upper right panel of Fig. 3. The distribution for the sum of near and far ℓ^- leptons is shown in the lower right panel. Its shape can easily be distinguished from the ℓ^+ results at large invariant masses.

Spin correlations are clearly important for the description of the invariant mass distributions; without taking spin correlations into account, all panels in Fig. 3 would be identical. Comparing the final distributions in the lower panels an asymmetry between positively and negatively charged leptons,

$$\mathcal{A} = \frac{\ell^+ - \ell^-}{\ell^+ + \ell^-}, \tag{3.5}$$

is predicted indeed [5]. (The asymmetry is washed out somewhat in pp collisions at the LHC where also antisquarks $\tilde{q}^*$ are produced; see Sec. III B). Figure 4 shows the parton-level asymmetry for the $\tilde{q}_L$ decay chain in SPS1a′. In particular for high invariant masses the dominance of positively charged leptons is evident. The NLO SQCD radiative corrections included in our decay analysis have a very small influence on the asymmetry. This is evident from the lower panel of Fig. 3; near the kinematic end point where the corrections to the invariant mass distribution of the positively charged lepton are biggest, the asymmetry is close to unity and changes are marginal as a result.

B. Squark cascade decays in pp collisions at the LHC

The more detailed numerical analysis presented in this final section is also based on the reference point SPS1a′ [12] in the minimal supergravity (mSUGRA) scenario.

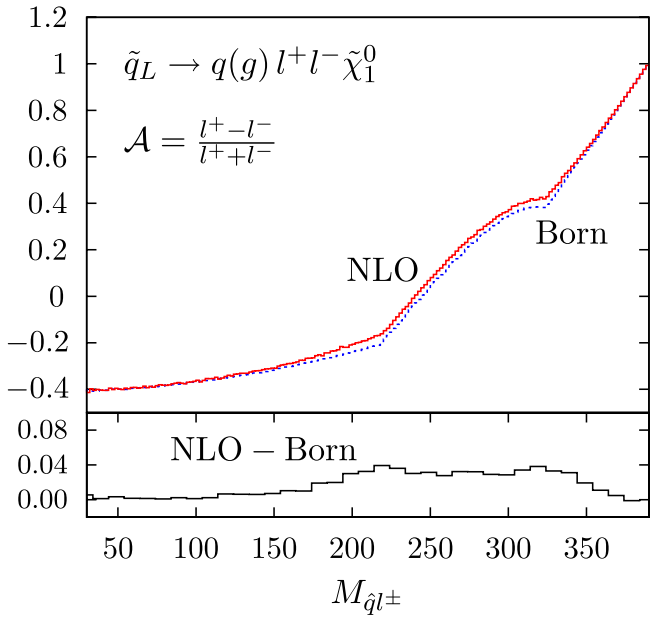

FIG. 4 (color online). The asymmetry Eq. (3.5) as a function of the $[\hat{q}l^\pm]$ invariant mass at SPS1a′ for $\tilde{q}_L$ decays (specifically for $\tilde{u}_L$ masses) into first and second generation lepton pairs (no antisquark decays included).

This point corresponds to the region of maximum probability in the analysis of electroweak precision observables [33,34] and it is compatible with the WMAP (Wilkinson Microwave Anisotropy Probe) measurement of the density of cold dark matter. The parameters of this mSUGRA scenario are defined as follows: gaugino mass $M_{1/2} = 250$ GeV, scalar mass $M_0 = 70$ GeV, and trilinear coupling $A_0 = -300$ GeV at the unification scale; moreover $\tan\beta = 10$ and $\mathrm{sign}(\mu) = +$. After evolution down to the Terascale the squark, gluino, slepton, and neutralino masses that will be used in the phenomenological analysis are collected in Table I, based on SUSPECT [35] with a difference of 1% to other programs, SPHENO [36] and SOFTSUSY [37].

Table I also presents the branching ratios which are based on NLO calculations as implemented in SUSYHIT [38] / SDECAY [39]. The L squarks decay predominantly into the charginos $\tilde{\chi}_1^\pm$ and the neutralino $\tilde{\chi}_2^0$. R-squarks decay almost exclusively into the $\tilde{\chi}_1^0$ LSP which is bino like. Hence, almost all of the squarks decaying to $\tilde{\chi}_2^0$ are indeed L-type squarks. Only a small admixture of R-type squarks diminishes the observed spin correlation and the asymmetry, Eq. (3.5), generated by the $\tilde{\chi}_2^0$ decay chain. More than half (i.e. 57%) of the neutralinos $\tilde{\chi}_2^0$ decay visibly into charged slepton-lepton pairs. Since left-handed sleptons of the first two generations are heavy, the decays are dominated (BR = 0.527) by decays into mixed $\tilde{\tau}_1$ states [40] with a reduced mass eigenvalue, but still a significant fraction decays to $\tilde{e}_R$, $\tilde{\mu}_R$ (BR = 0.024 for each mode). If the e, μ leptonic decays are used as experimental signals, the transverse momenta of the cascading $\tau \to e$, μ final states are strongly reduced. A large fraction of the $\tau \to e$, μ decay events will thus be lost in experimental cuts, about 90% for a transverse momentum cut of 10 GeV.

Since experiments will not distinguish quark from antiquark jets, experimentally observed distributions will also receive contributions from antisquark decay chains. For antisquarks, by CP invariance, the role of positively and negatively charged leptons is interchanged and the asymmetry $\mathcal{A}$ is reduced as a result. At the Tevatron, the equal rate for squark and antisquark production drives $\mathcal{A}$ even to zero. However, the (non-CP-invariant) proton-proton initial state at the LHC ensures that more squarks than antisquarks are produced and a nonzero asymmetry is predicted.

At the LHC, squarks are produced either directly in quark/antiquark/gluon collisions, or they are decay products of gluinos as $M_{\tilde{g}} > M_{\tilde{q}}$ for the SPS1a′ reference point. The production cross sections for both species have been determined including the next-to-leading order corrections of Ref. [41] as implemented in PROSPINO [42]. The NLO calculation of Ref. [41] has been performed for mass-degenerate L and R squarks and mass-degenerate first and second generation squarks of up and down type. Since the mass differences are in general small, in particular, for the spectrum of the SPS1a′ reference point where $[M_L^2 - M_R^2]/[M_L^2 + M_R^2] \approx 4\%$, this is a valid approximation. In our tree-level calculation, to which we apply the K-factors, the exact kinematics is used. For the parton densities the CTEQ5 set [43] has been adopted and the renormalization and factorization scales have been set to the average mass of the produced particles. The production cross sections are displayed, exemplarily for squarks and antisquarks of the first generation, in Table II. The pp initial state at the LHC clearly favors the direct production of squarks over the direct production of antisquarks. Though equal numbers of squarks and antisquarks are generated by gluino decays, the ratio of the number of antisquarks over squarks is only slightly diminished because the branching ratio of gluinos into first and second generation L squarks is small.

TABLE I. Masses and decay branching ratios most relevant for evaluating the SPS1a′ squark/gluino cascades.

	Mass [GeV]	BR($[\tilde{g} \to]\tilde{q} \to \tilde{\chi}_2^0$) [%]
$\tilde{u}_L$	558	32.2
$\tilde{d}_L$	564	31.6
$\tilde{u}_R$	542	0.6
$\tilde{d}_R$	542	0.6
$\tilde{g}$	605	$\tilde{u}_L/\tilde{d}_L$: 0.8/0.6
		$\tilde{u}_R/\tilde{d}_R$: 0.03/0.03

	Mass [GeV]	BR($\tilde{\chi}_2^0 \to \tilde{l}$) [%]
$\tilde{\chi}_1^0$	98	
$\tilde{\chi}_2^0$	183	$\tilde{e}_R^+$: 1.2
		$\tilde{\tau}_1^+$: 26.4
$\tilde{e}_R$	124	
$\tilde{\tau}_1$	108	

TABLE II. Cross sections for the production of squarks of the first generation and gluino production in pp collisions at the LHC, and the production cross sections for the neutralino $\tilde{\chi}_2^0$ in the cascades. Also shown are the cross sections for R-sleptons after summing up all cascade channels. The resulting cross sections for electron/muon pairs from direct electron/muon production in the decay chain and from tau decays are collected in the right-most column.

	$\sigma(pp \to \tilde{q}/\tilde{g})$ [pb]	$\sigma(\tilde{q}/\tilde{g} \to \tilde{\chi}_2^0)$ [pb]
$\tilde{u}_L/\tilde{u}_R$	14.4/15.4	4.6/0.1
$\tilde{d}_L/\tilde{d}_R$	6.7/7.4	2.1/0.05
$\tilde{u}_L^*/\tilde{u}_R^*$	1.7/1.9	0.6/0.01
$\tilde{d}_L^*/\tilde{d}_R^*$	2.0/2.3	0.6/0.01
$\tilde{g}$	45.1	2.6

	$\sigma(\tilde{l}_R)$ [pb]	$\sigma(e, \mu)$ [pb]
$\tilde{e}_R + \tilde{\mu}_R$	0.57	0.57
$\tilde{\tau}_1$	6.37	0.39

Table II also includes the cross sections times branching ratios $\sigma(\tilde{q}) \times \mathrm{BR}(\tilde{q} \to \chi_2^0)$ and $\sigma(\tilde{g}) \times \mathrm{BR}(\tilde{g} \to \tilde{q} \to \chi_2^0)$ for neutralino $\tilde{\chi}_2^0$ production from squark decays, and the final cross sections times branching ratios for the signal $\sigma[e, \mu]$, i.e. lepton production from squark cascades of the first two generations, with τ decays separated. With a nominal integrated luminosity of 300 fb^{-1}, a sample of roughly $2 \cdot 10^5$ events is accumulated for the SPS1a′ benchmark for e, μ in the first two generations and, before experimental cuts, an initial number of $1.5 \cdot 10^5$ τ events decaying leptonically into either electrons or muons. Although these calculations are of a purely theoretical nature, they provide nevertheless a solid platform for estimating expectations before experimental simulations will finally include selection cuts, efficiencies, etc.

Using these estimates of production cross sections and branching ratios, the invariant mass distributions for the SPS1a′ decay chain can be calculated. Figure 5 displays the LO and NLO [jet$\ell^{\pm}$] invariant mass spectrum for positively and negatively charged leptons as predicted for the LHC. The distributions are normalized to the signal cross sections and are shown separately for $\tilde{\chi}_2^0$ decays to first/second generation leptons/sleptons and for $\tau/\tilde{\tau}$ decaying leptonically. L/R mixing of the τ sleptons and the $\tilde{\chi}_2^0$ Higgsino component exacerbate the analysis of the $\tau/\tilde{\tau}$ channel considerably; all these effects have been taken into account in the numerical analysis. However, the leptonic τ decay signal is strongly reduced to a level of 10% if a transverse momentum cut of 10 GeV is applied as indicated by the dotted lines. (For simplicity, the cut is applied in the squark rest frame. This approximation is adequate since squarks are produced predominantly at small velocities.) The experimentally observable distributions are clearly distinct despite the antisquark admixture to the squark sample. As a result of the antisquark admixture, the ℓ^+/ℓ^- asymmetry (3.5) is slightly reduced at the LHC compared with Fig. 4 for pure $\tilde{q}_L$ decays, with marginal NLO corrections as before. However, the asymmetry is still quite significant for large [jetℓ] invariant masses as demonstrated in Refs. [5–7], even after including detector effects.

IV. CONCLUSIONS

Edges/thresholds, distributions, and correlations of particles in cascades play an important role in determining properties of supersymmetric particles, i.e. masses and spins. Lepton-lepton and jet-lepton invariant mass distributions are particularly useful instruments in this context.

In the present article we have studied how the parton final states in $\tilde{q} \to q\tilde{\chi}$ decays are affected by super-QCD corrections at next-to-leading order, in particular, by the radiation of gluons in the decay process. The corrections modify the energy as well as the polarization of the particles. By performing an analytic next-to-leading order analysis we have provided a detailed understanding of origin and size of these effects. Moreover, we have studied particular decay channels and [jet$\ell^{\pm}$] invariant mass distributions, exemplified for the SPS1a′ benchmark scenario, in $\tilde{q}_L \to q\ell^+\ell^-\tilde{\chi}_1^0$ decays. We have found significant gluonic corrections to the shape of the invariant [jetℓ^+] mass distribution near the pronounced edge at the kinematic end point.

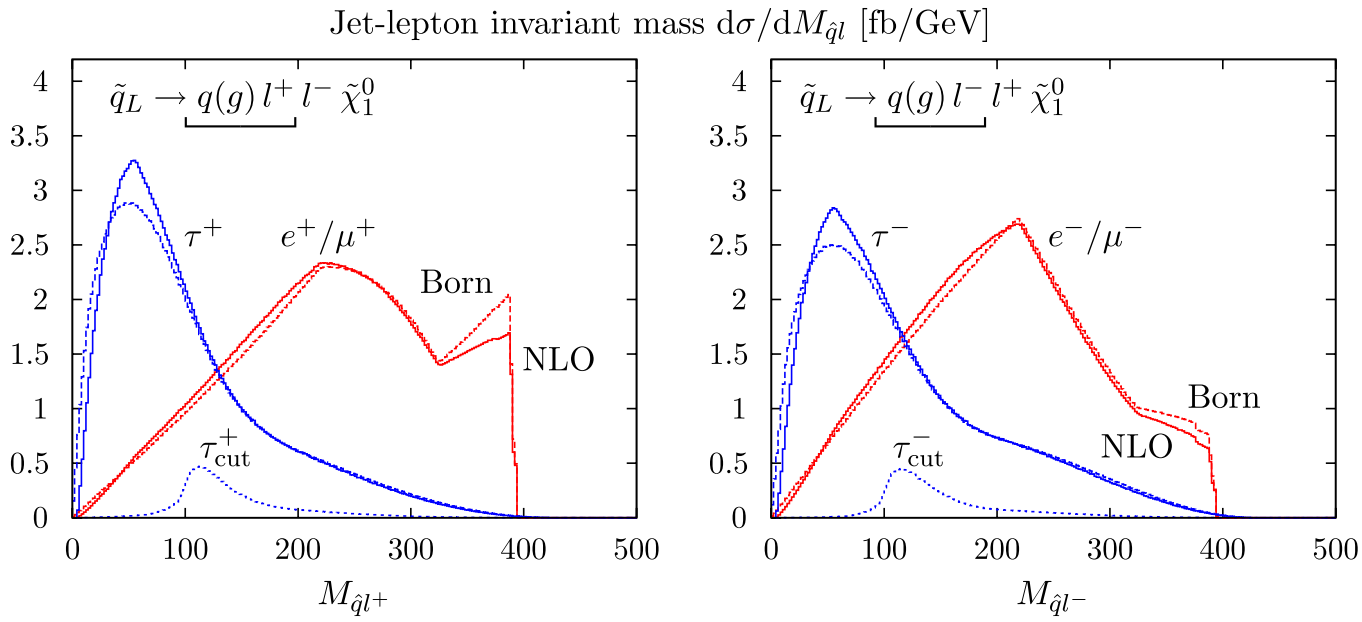

FIG. 5 (color online). Invariant [$\hat{q}l$] mass distributions, $y_c = 0.01$, for muons and electrons produced directly in the neutralino and slepton decay. For muon and electron pairs produced from tau decays in the decay chain, the reduction of the NLO cross sections for a transverse momentum cut of 10 GeV is indicated by the dotted lines.

ACKNOWLEDGMENTS

We gratefully acknowledge communications with G. Polesello, and D. J. Miller, P. Osland and A. R. Raklev. We are thankful to A. Djouadi for comments on the manuscript. This work was supported in part by the DFG SFB/TR9 "Computational Particle Physics," and by the European Community's Marie-Curie Research Training Network HEPTOOLS under Contract No. MRTN-CT-2006-035505. P. M. Z. thanks the LPT and the Institut für Theoretische Physik E for the warm hospitality extended to him at the Université Paris-Sud and at the RWTH Aachen.

[1] I. Hinchliffe, F. E. Paige, M. D. Shapiro, J. Soderqvist, and W. Yao, Phys. Rev. D **55**, 5520 (1997).
[2] B. C. Allanach, C. G. Lester, M. A. Parker, and B. R. Webber, J. High Energy Phys. 09 (2000) 004.
[3] B. K. Gjelsten, D. J. Miller, and P. Osland, J. High Energy Phys. 12 (2004) 003.
[4] G. Weiglein *et al.* (LHC/LC Study Group), Phys. Rep. **426**, 47 (2006).
[5] A. J. Barr, Phys. Lett. B **596**, 205 (2004).
[6] J. M. Smillie and B. R. Webber, J. High Energy Phys. 10 (2005) 069.
[7] C. Athanasiou, C. G. Lester, J. M. Smillie, and B. R. Webber, J. High Energy Phys. 08 (2006) 055.
[8] L. T. Wang and I. Yavin, J. High Energy Phys. 04 (2007) 032.
[9] B. K. Gjelsten, D. J. Miller, P. Osland, and A. R. Raklev, AIP Conf. Proc. **903**, 257 (2007).
[10] R. Kitano and Y. Nomura, Phys. Rev. D **73**, 095004 (2006).
[11] D. J. Miller, P. Osland, and A. R. Raklev, J. High Energy Phys. 03 (2006) 034; D. J. Miller, P. Osland, and A. R. Raklev (private communication).
[12] B. C. Allanach *et al.*, Eur. Phys. J. C **25**, 113 (2002).
[13] J. A. Aguilar-Saavedra *et al.*, Eur. Phys. J. C **46**, 43 (2006).
[14] W. Beenakker, R. Höpker, and P. M. Zerwas, Phys. Lett. B **378**, 159 (1996).
[15] K.-i. Hikasa and Y. Nakamura, Z. Phys. C **70**, 139 (1996); **71**, 356(E) (1996).
[16] S. Kraml, H. Eberl, A. Bartl, W. Majerotto, and W. Porod, Phys. Lett. B **386**, 175 (1996).
[17] A. Djouadi, W. Hollik, and C. Jünger, Phys. Rev. D **55**, 6975 (1997).
[18] W. Beenakker, R. Höpker, T. Plehn, and P. M. Zerwas, Z. Phys. C **75**, 349 (1997).
[19] S. Y. Choi, A. Djouadi, M. Guchait, J. Kalinowski, H. S. Song, and P. M. Zerwas, Eur. Phys. J. C **14**, 535 (2000).
[20] S. Y. Choi, J. Kalinowski, G. A. Moortgat-Pick, and P. M. Zerwas, Eur. Phys. J. C **22**, 563 (2001); **23**, 769(E) (2002).
[21] G. Schierholz, *SLAC Summer Institute on Particle Physics* (Stanford, California, 1979), SLAC Summer Institute 1979:0476.
[22] P. Binetruy, Phys. Lett. **91B**, 245 (1980).
[23] S. Catani, G. Turnock, B. R. Webber, and L. Trentadue, Phys. Lett. B **263**, 491 (1991).
[24] T. Plehn, H. Spiesberger, M. Spira, and P. M. Zerwas, Z. Phys. C **74**, 611 (1997).
[25] The integrals are defined as $K(z) = \int_0^{\pi/2}(1 - z\sin^2 x)^{-1/2}dx$ and $E(z) = \int_0^{\pi/2}(1 - z\sin^2 x)^{1/2}dx$.
[26] P. Richardson, J. High Energy Phys. 11 (2001) 029.
[27] G. Sterman and S. Weinberg, Phys. Rev. Lett. **39**, 1436 (1977).
[28] A. Heister *et al.* (ALEPH Collaboration), Eur. Phys. J. C **35**, 457 (2004).
[29] The accuracy of the narrow-width approximation for cascade decays has been addressed in Ref. [30].
[30] N. Kauer, J. High Energy Phys. 04 (2008) 055.
[31] Electroweak radiative corrections to the decay $\tilde{\chi}_2^0 \to l^+ l^- \tilde{\chi}_1^0$ have been presented in Ref. [32].
[32] M. Drees, W. Hollik, and Q. Xu, J. High Energy Phys. 02 (2007) 032.
[33] B. C. Allanach, K. Cranmer, C. G. Lester, and A. M. Weber, J. High Energy Phys. 08 (2007) 023.
[34] J. R. Ellis, S. Heinemeyer, K. A. Olive, A. M. Weber, and G. Weiglein, J. High Energy Phys. 08 (2007) 083.
[35] A. Djouadi, J. L. Kneur, and G. Moultaka, Comput. Phys. Commun. **176**, 426 (2007).
[36] W. Porod, Comput. Phys. Commun. **153**, 275 (2003).
[37] B. C. Allanach, Comput. Phys. Commun. **143**, 305 (2002).
[38] A. Djouadi, M. M. Mühlleitner, and M. Spira, Acta Phys. Pol. B **38**, 635 (2007).
[39] M. Mühlleitner, A. Djouadi, and Y. Mambrini, Comput. Phys. Commun. **168**, 46 (2005).
[40] S. Y. Choi, K. Hagiwara, Y. G. Kim, K. Mawatari, and P. M. Zerwas, Phys. Lett. B **648**, 207 (2007).
[41] W. Beenakker, R. Höpker, M. Spira, and P. M. Zerwas, Nucl. Phys. **B492**, 51 (1997).
[42] The PROSPINO computer code can be obtained from http://www.ph.ed.ac.uk/~tplehn/prospino/ or from http://people.web.psi.ch/spira/prospino/.
[43] H. L. Lai *et al.* (CTEQ Collaboration), Eur. Phys. J. C **12**, 375 (2000).